JHEP PROCEEDINGS

International Workshop on Astroparticle and High Energy Physics

A phenomenological approach to neutrino oscillations

G.L. Fogli*, **E. Lisi**, **A. Marrone**, **A. Palazzo**, **A.M. Rotunno**

Dipartimento di Fisica and Sezione INFN, Via Amendola 173, I-70126 Bari

D. Montanino

Dipartimento di Scienza dei Materiali and Sezione INFN, Via Arnesano, 73100 Lecce

ABSTRACT: We review the status of the neutrino oscillations physics, with a particular emphasis on the present knowledge of the neutrino mass-mixing parameters. We consider first the $\nu_\mu \to \nu_\tau$ flavor transitions of atmospheric neutrinos. It is found that standard oscillations provide the best description of the SK+K2K data, and that the associated mass-mixing parameters are determined at $\pm 1\sigma$ (and $N_{\rm DF} = 1$) as: $\Delta m^2 = (2.6 \pm 0.4) \times 10^{-3}$ eV^2 and $\sin^2 2\theta = 1.00^{+0.00}_{-0.05}$. Such indications, presently dominated by SK, could be strengthened by further K2K data. Then we point out that the recent data from the Sudbury Neutrino Observatory, together with other relevant measurements from solar and reactor neutrino experiments, in particular the KamLAND data, convincingly show that the flavor transitions of solar neutrinos are affected by Mikheyev-Smirnov-Wolfenstein (MSW) effects. Finally, we perform an updated analysis of two-family active oscillations of solar and reactor neutrinos in the standard MSW case.

1. Introduction

In its first phase of operation (years 1996–2001), the Super-Kamiokande (SK) experiment has provided, among other important results, compelling evidence for atmospheric ν_μ disappearance [1, 2]. This evidence, now firmly based on a high-statistics 92 kton-year exposure [3], has not only been corroborated by consistent indications in the MACRO [4] and Soudan 2 [5] atmospheric neutrino experiments, but has also been independently checked by the first long-baseline KEK-to-Kamioka (K2K) accelerator experiment [6, 7], using SK as a target for ν_μ's produced 250 km away with $\langle E_\nu \rangle \sim 1.3$ GeV. Neutrino flavor oscillations, interpreted in terms of nonzero mass-mixing parameters $(\Delta m^2, \sin^2 2\theta)$ in the $\nu_\mu \to \nu_\tau$ channel, provide by far the best and most natural explanation for the observed ν_μ disappearance [1, 2].

*Speaker.

In Section 2 we review the phenomenological status of the standard oscillations in the $\nu_\mu \to \nu_\tau$ channel, in the light of the latest SK atmospheric zenith distributions [3] and of the first spectral results from the K2K experiment [7].

On the solar neutrino front, the Sudbury Neutrino Observatory (SNO) experiment has recently released new data [8] with enhanced sensitivity to neutral-current (NC) interactions of solar neutrinos in deuterium. Charged current (CC) and elastic scattering (ES) events have also been statistically separated from NC events in a model-independent way, i.e., without using priors on the ^{8}B neutrino energy spectrum shape [8]. These data corroborate the explanation of the solar neutrino deficit in terms of (dominant) two-family $\nu_e \to \nu_a$ flavor transitions ($\nu_a = \nu_{\mu,\tau}$), which have convincingly emerged from the combined data of previous solar neutrino experiments (Chlorine [9], Gallium [10, 11, 12], Super-Kamiokande (SK) [13, 14], and SNO [15, 16, 17]) and of long-baseline reactor oscillation searches at KamLAND [18]. Moreover, the new SNO data appear to forbid relatively high values of the neutrino mixing angle θ_{12} (close to maximal mixing) and of the squared mass difference δm^2 (close to the CHOOZ [19] upper bound), which were marginally allowed prior to [8] (see, e.g., [20, 21]). In the current global fit, the mass-mixing parameters appear to be tightly confined in the so-called large mixing angle (LMA) region, and especially in a subregion often denoted as LMA-I [20].

In the LMA parameter range, flavor transitions between ν_e and ν_a should be significantly affected by the neutrino interaction energy difference $V = V_e - V_a$ arising in solar (and possibly Earth) background matter [22, 23],

$$V(x) = \sqrt{2} G_F N_e(x) \ , \tag{1.1}$$

where N_e is the electron number density at the point x. The associated flavor change, known as Mikheyev-Smirnov-Wolfenstein (MSW) effect [22], should occur adiabatically [24] in the solar matter, for LMA parameters. In the context of Hamiltonian ($\mathcal{H}$) evolution of 2ν active flavors, the MSW effect enters through a dynamical term $\mathcal{H}_{\rm dyn}$ in matter, in addition to the kinetic term $\mathcal{H}_{\rm kin}$ in vacuum:

$$i \frac{d}{dx} \begin{pmatrix} \nu_e \\ \nu_a \end{pmatrix} = (\mathcal{H}_{\rm dyn} + \mathcal{H}_{\rm kin}) \begin{pmatrix} \nu_e \\ \nu_a \end{pmatrix} \ , \tag{1.2}$$

where

$$\mathcal{H}_{\rm dyn} = \frac{V(x)}{2} \begin{pmatrix} 1 & 0 \\ 0 & -1 \end{pmatrix} \tag{1.3}$$

and

$$\mathcal{H}_{\rm kin} = \frac{\delta m^2}{4E} \begin{pmatrix} -\cos 2\theta_{12} & \sin 2\theta_{12} \\ \sin 2\theta_{12} & \cos 2\theta_{12} \end{pmatrix} \ , \tag{1.4}$$

E being the neutrino energy.

In a previous recent work [25] we pointed out that, while the evidence for $\mathcal{H}_{\rm kin} \neq 0$ was overwhelming, the phenomenological indications in favor of $\mathcal{H}_{\rm dyn} \neq 0$ (and thus of MSW effects) were not as compelling. In particular, we introduced in [25] a free parameter $a_{\rm MSW}$

modulating the overall amplitude of the dynamical term $\mathcal{H}_{\rm dyn}$ through the substitution

$$V \to a_{\rm MSW} \cdot V \ , \tag{1.5}$$

both in the Sun and in the Earth. We showed that $a_{\rm MSW}$ was poorly constrained, despite an intriguing preference for the standard MSW expectation $a_{\rm MSW} \sim 1$ [25]. The null hypothesis $a_{\rm MSW} = 0$ was not clearly disproved by any single experiment, and could be rejected at a relevant confidence level ($\Delta\chi^2 \simeq 13$, formally equivalent to $\sqrt{\Delta\chi^2} \simeq 3.5\sigma$) only in the global fit. We concluded that the available phenomenological data clearly favored MSW effects in solar neutrinos, but did not prove unequivocally their occurrence. We deemed it necessary to wait for new KamLAND or SNO data, in order to clarify the situation and to probe MSW effects with higher statistical significance [25].

In this work, we point out that the recent SNO data [8] contribute significantly to disprove the null hypothesis of no MSW oscillations. In the global combination of solar and reactor data, we find that, with respect to the (preferred) standard case $a_{\rm MSW} \sim 1$, the null hypothesis $a_{\rm MSW} = 0$ can be safely rejected at the level of $\sim 5.6\sigma$, despite the fact the allowed range of $a_{\rm MSW}$ is still rather large. In other words, the evidence in favor of MSW effects is now very strong, although precision tests of the MSW physics cannot be performed until new, high statistics KamLAND data become available (as we show later).

In Section 3, we analyze the current solar and reactor neutrino phenomenology with an increasing degree of dependence on assumptions about the MSW effect.[1] In Subsec. 3.1 we do not make any hypothesis about MSW effects, and show that SNO data alone, as well as a model-independent SNO+SK combination, constrain the energy-averaged ν_e survival probability $\langle P_{ee} \rangle$ to be significantly smaller than 1/2. This fact, by itself, excludes the vacuum case $a_{\rm MSW} = 0$ (which would predict $\langle P_{ee} \rangle \geq 1/2$ in the LMA region selected by KamLAND), and proves that dynamical effects *must* occur in solar neutrino propagation with unspecified amplitude $a_{\rm MSW} > 0$. In Subsec. 3.2 we fit all the available solar and reactor data with $(\delta m^2, \theta_{12}, a_{\rm MSW})$ taken as free parameters. We find that MSW effects with standard amplitude ($a_{\rm MSW} = 1$) are favored, while the null hypothesis ($a_{\rm MSW} = 0$) can be safely rejected at the $\sim 5.6\sigma$ level. However, we show that the allowed range of $a_{\rm MSW}$ is still very large, and can be significantly narrowed only by future KamLAND data. Assuming standard MSW effects ($a_{\rm MSW} = 1$), we perform in Subsec. 3.3 an updated analysis of the 2ν kinematical parameters $(\delta m^2, \sin^2\theta_{12})$. We briefly discuss the impact of 3ν mixing in Sec. 4, and conclude our work in Sec. 5.

2. "Atmospheric" neutrinos

A careful analysis of the SK and K2K data sets used in the following can be found in [26]. Concerning SK atmospheric neutrino data (92 kton-year [3]), we use the usual zenith angle (θ_z) distributions of leptons: sub-GeV e-like and μ-like events, divided in 10+10 bins; multi-GeV e-like and μ-like events, divided in 10+10 bins; upward stopping and through-going μ events, divided in 5+10 bins. The calculation of the theoretical events rates $R_n^{\rm theo}$

[1] In any case, we assume active flavor oscillations only, and discard hypothetical sterile neutrinos.

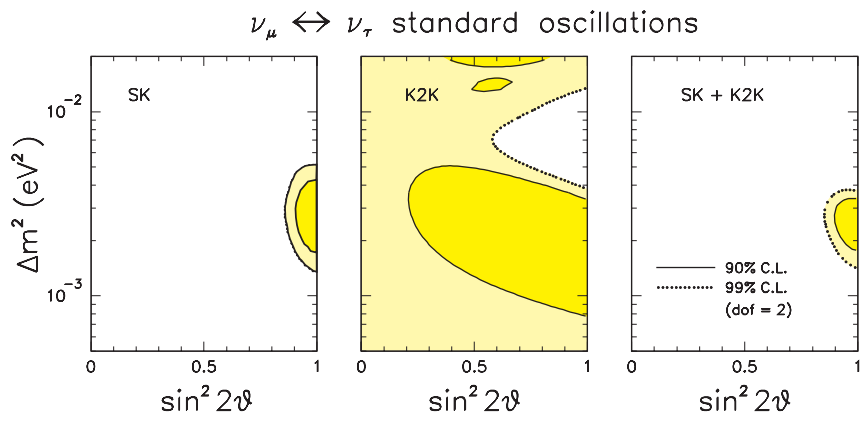

Figure 1: Standard oscillations in the $\nu_\mu \to \nu_\tau$ channel: bounds on the parameters $(\Delta m^2, \sin^2 2\theta)$ from SK atmospheric data (left panel), K2K spectral data (middle panel), and their combination (right panel).

in each of the 55 bins is done as in [27, 28, 29]. The SK statistical analysis is considerably improved with respect to [27, 29]. Now the set of systematic errors has been enlarged to 11 entries, leading to a more complex structure of correlated errors affecting the $R_n^{\rm theo}$'s, as emphasized in [30].

Concerning the K2K data, we use the absolute spectrum of muon events in terms of the reconstructed neutrino energy E [7], which provides a total of 29 events (here divided in 6 bins). In this sample, the parent neutrino interactions are dominantly quasi-elastic (QE), and the reconstructed energy E is thus closely correlated with the true neutrino energy E_ν.

Let us now discuss the updated bounds on the parameters $(\Delta m^2, \sin^2 2\theta)$, governing the scenario of standard oscillations.

Figure 1 shows the joint bounds on the $(\Delta m^2, \sin^2 2\theta)$ parameters from our analysis of SK, K2K, and SK+K2K data. The bounds in the left panel are very close to the official SK ones, as presented in [3]. The bounds in the middle panel are instead slightly weaker than the official K2K ones [7], especially in terms of $\sin^2 2\theta$. In particular, we do not find a lower bound on $\sin^2 2\theta$ at 99% C.L. (for $N_{\rm DF} = 2$). The reason is that we cannot use the additional (dominantly) non-QE event sample of K2K (27 events), which would help to constrain the overall rate normalization and thus $\sin^2 2\theta$. This fact might also explain why we find the K2K best fit at $\sin^2 2\theta = 0.82$ rather than at 1.00 as in [7]. By comparing left and right panels of Fig. 1, the main effect of K2K appears to be the strengthening of the upper bound on Δm^2, consistently with the trend of the first K2K data (rate only [6], no spectrum) [29]. The main reason is that, for $\Delta m^2 \sim (4\text{–}6) \times 10^{-3}$ eV^2, the first oscillation minimum would be located at—or just above—the K2K energy spectrum peak, implying a strong local and overall suppression of the expected events.

Figure 2 shows on the left the SK and SK+K2K bounds on Δm^2, when the $\sin^2 2\theta$ parameter is projected (minimized) away. The linear scale in Δm^2 makes the K2K impact on the upper limit more evident. Notice that, up to $\sim 3\sigma$, the global (SK+K2K) χ^2 function is approximately parabolic in the *linear* variable Δm^2, so that one can define a

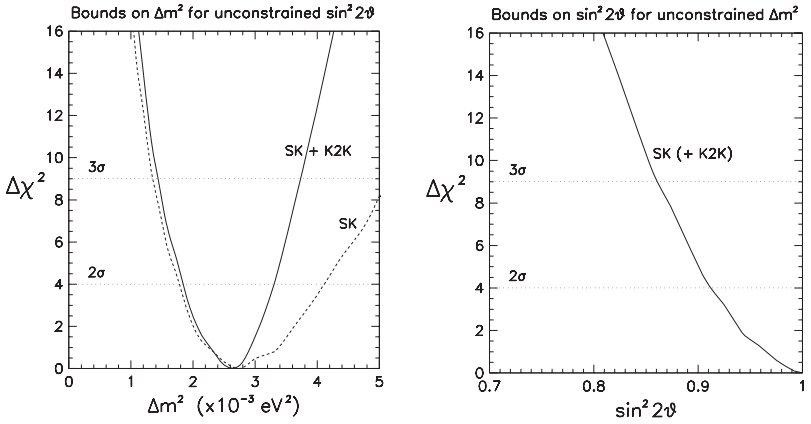

Figure 2: Standard oscillations in the $\nu_\mu \to \nu_\tau$ channel. On the left: bounds on Δm^2 for unconstrained $\sin^2 2\theta$ from SK (dashed curve) and SK+K2K (solid curve). On the right: bounds on $\sin^2 2\theta$ for unconstrained Δm^2 from SK data. The inclusion of K2K data induces here negligible changes (not shown).

one- standard-deviation error for this parameter. This feature, here confirmed through a full analysis, was already argued on the basis of a graphical reduction of the official SK and K2K likelihood functions [31]. By keeping only the first significant figure in the error estimate, a parabolic fit provides the $\pm 1\sigma$ range,

$$\Delta m^2 = (2.6 \pm 0.4) \times 10^{-3} \text{ eV}^2 \ . \tag{2.1}$$

The bounds on $\sin^2 2\theta$ are instead entirely dominated by SK. This is shown on the right of Fig. 3, where the $\Delta\chi^2$ function in terms of $\sin^2 2\theta$ is reported, for Δm^2 projected (minimized) away in the SK fit. Here the addition of K2K data would insignificantly change the bounds (not shown), which thus hold for both the SK and the SK+K2K fit. Also in this case, the nearly parabolic behavior of $\Delta\chi^2$ allows to properly define a 1σ range,

$$\sin^2 2\theta = 1.00^{+0.00}_{-0.05} \ , \tag{2.2}$$

with the lower $N\sigma$ error scaling linearly with N (up to $N \simeq 3$).Equations (2.1) and (2.2) concisely review the current fit to the standard oscillation parameters, as anticipated in the Introduction.

Figure 3 shows the comparison between observations and best-fit predictions for the SK zenith distributions. In particular, the comparison between solid and dashed histograms shows that systematic shifts are often comparable in size to statistical errors, implying that just increasing the SK atmospheric ν statistics will hardly bring decisive new information on the standard oscillation scenario. In the SG and MG samples, the fit clearly exploits the systematic uncertainties to increase the e-like event normalization, especially in the upward direction, so as to reduce the "electron excess" possibly indicated by SK data.

Concerning μ-like events in the SG and MG samples, the fit shows an opposite tendency to slightly decrease the normalization of (especially down-going) events. The tendency appears to be reversed in the high-energy UT sample. Taken together, these opposite

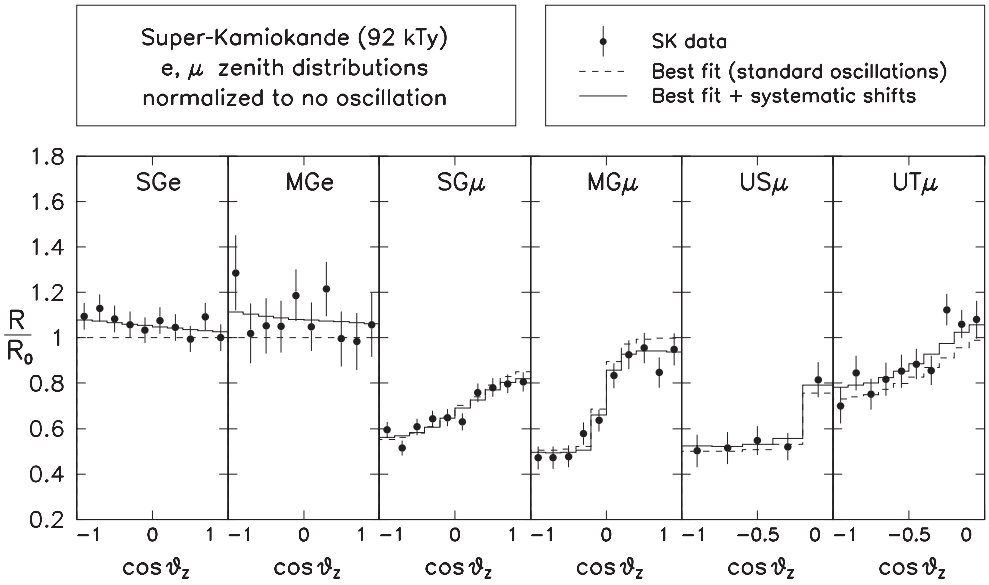

Figure 3: SK experimental zenith distributions ($\pm 1\sigma_{\rm stat}$), compared with the corresponding theoretical ones at the global (SK+K2K) best-fit point. All distributions are normalized to the unoscillated predictions in each bin. For the theoretical event rates, we show both the central values $R_n^{\rm theo}$ (dashed histograms) and the "shifted" values $\overline{R}_n^{\rm theo}$ (solid histograms), which embed the effect of systematic pulls. The difference between $\overline{R}_n^{\rm theo}$ and $R_n^{\rm theo}$ shows how much (and in which direction) the correlated systematic errors tend to stretch the predictions in order to match the data.

shifts of e-like and μ-like expectations in the SG and MG samples seem to suggest some systematic deviation from the predicted μ/e flavor ratio which, although not statistically alarming, should be kept in mind: deviations of similar size might have their origin in neutrino physics beyond 2ν oscillations. Unfortunately, since such effects are typically not larger than the systematic shifts in Fig. 3, they are likely to remain hidden in higher-statistics SK data.

3. Solar neutrinos (a 2ν analysis)

3.1 Model-independent constraints

It has been shown in [32] (see also [30]) that the SK and SNO experiments probe the same energy-averaged ν_e survival probability $\langle P_{ee} \rangle$ to a good accuracy, provided that the detector thresholds are appropriately chosen. For the kinetic energy threshold ($T_{\rm SNO} = 5.5$ MeV) and energy resolution characterizing the latest SNO data [8], we find that the equivalent SK threshold is $E_{\rm SK} \simeq 7.8$ MeV in total energy. For equalized thresholds, the SK ES flux and the SNO NC and CC fluxes are linked by the *exact* relations [32]

$$\Phi_{\rm ES}^{\rm SK} = \Phi_B[\langle P_{ee} \rangle + r(1 - \langle P_{ee} \rangle)] \; , \tag{3.1}$$

$$\Phi_{\rm CC}^{\rm SNO} = \Phi_B \langle P_{ee} \rangle \; , \tag{3.2}$$

$$\Phi_{\rm NC}^{\rm SNO} = \Phi_B \; , \tag{3.3}$$

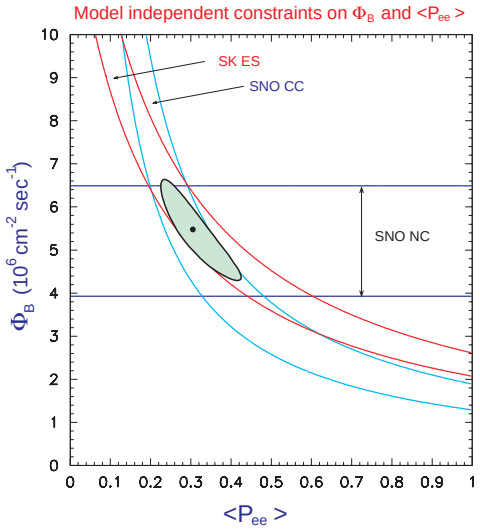

Figure 4: Results of the model-independent analysis of SNO (CC and NC) and SK (ES) neutrino fluxes. The projections of the ellipse provide 3σ bounds on the ^{8}B neutrino flux Φ_B and on the energy-averaged ν_e survival probability $\langle P_{ee} \rangle$.

where $r = 0.154$ is the ratio of (properly averaged) $\nu_{\mu,\tau}$ and ν_e CC cross sections, and Φ_B is the true ^{8}B flux from the Sun. From the above equations, one can (over)constrain both Φ_B and $\langle P_{ee} \rangle$ in a truly model-independent way, namely, without any prior assumption about the energy profile of P_{ee} or about Φ_B predictions in standard solar models (SSM).

Figure 4 shows the current constraints on Φ_B and on $\langle P_{ee} \rangle$ as derived from the final SK ES data [13] and from the latest SNO CC and NC fluxes [8] (correlations included [33]). The constraints are shown both by individual bands and by their combination at the 3σ level ($\Delta\chi^2 = 9$). The projections of the SNO+SK combination (the ellipse in Fig. 4) provide the range

$$\Phi_B = (5.5 \pm 1.2) \times 10^6 \text{ cm}^{-2}\text{s}^{-1} \ (3\sigma) \ , \tag{3.4}$$

in good agreement with SSM predictions [34], and

$$\langle P_{ee} \rangle = 0.31^{+0.12}_{-0.08} \ (3\sigma) \ . \tag{3.5}$$

The above 3σ limits on $\langle P_{ee} \rangle$ are in very good agreement with the "3σ range" obtained by naively triplicating the errors of the SNO CC/NC flux ratio, which is a direct measurement of $\langle P_{ee} \rangle$: $\Phi_{\text{CC}}^{\text{SNO}}/\Phi_{\text{NC}}^{\text{SNO}} = 0.306 \pm 0.105 (3\sigma)$ [8]. However, as emphasized in [33], the errors of the CC/NC ratio are not normally distributed, and should not be used in fits. Conversely, our bounds in Eq. (3.5) are statistically safe and well-defined, and will be used in the following discussion.

The above SK+SNO constraints appear to be currently dominated by the SNO data. In particular, the upper bound on the ν_e survival probability,

$$\langle P_{ee} \rangle < 0.43 \ (3\sigma) \ , \tag{3.6}$$

can be basically derived from the SNO (CC+NC) data [8] alone. The upper limit in Eq. (3.6) is significantly stronger than the one derived in[30], prior to the latest SNO data

[8]. In particular, we have now robust, model-independent evidence that P_{ee} is definitely smaller than 1/2 at $> 3\sigma$ level. This inequality has important consequences for both the dynamical and the kinematical term in Eq. (1.2). First, in the δm^2 range accessible to KamLAND and below the CHOOZ bound ($\delta m^2 \sim O(10^{-4\pm1})$ eV^2), the absence of the dynamical MSW term $\mathcal{H}_{\rm dyn}$ (i.e., the case $a_{\rm MSW} = 0$ would imply $\langle P_{ee} \rangle \geq 1/2$ (see, e.g,[25]), contrary to Eq. (3.6) . Second, assuming standard MSW dynamics ($a_{\rm MSW} = 1$), the inequality in Eq. (3.6) allows to place upper limits on the kinematical parameters δm^2 and $\sin^2\theta_{12}$ (see, e.g., the discussions in [25, 35, 36]).

Summarizing, the latest SNO CC and NC data [8], either by themselves or in combination with the SK ES data [14], provide the strong, model-independent upper bound $\langle P_{ee} \rangle < 0.43$ at 3σ. In the context of 2ν mixing, and within the mass-mixing region probed by KamLAND, this bound allows to reject the null hypothesis ($a_{\rm MSW} = 0$), and provides upper limits on the mass-mixing parameters in the standard MSW case ($a_{\rm MSW} = 1$). In the next Section, we examine the more general case of variable $a_{\rm MSW}$, in order to test whether current and future data can significantly constrain, by themselves, the size of matter effects.

3.2 Constraints on the MSW dynamical term

In this subsection we present the results of a global analysis of solar and reactor (KamLAND + CHOOZ) data with $(\delta m^2, \sin^2\theta_{12}, a_{\rm MSW})$ unconstrained. The latest SNO data [8] are incorporated according to the recommendations in [33]. The reader is referred to [25] for other details of the analysis.

Figure 5 shows the results of the global χ^2 fit, in terms of the function $\Delta\chi^2(a_{\rm MSW})$ after $(\delta m^2, \sin^2\theta_{12})$ marginalization. Such marginalization is appropriate to test the size

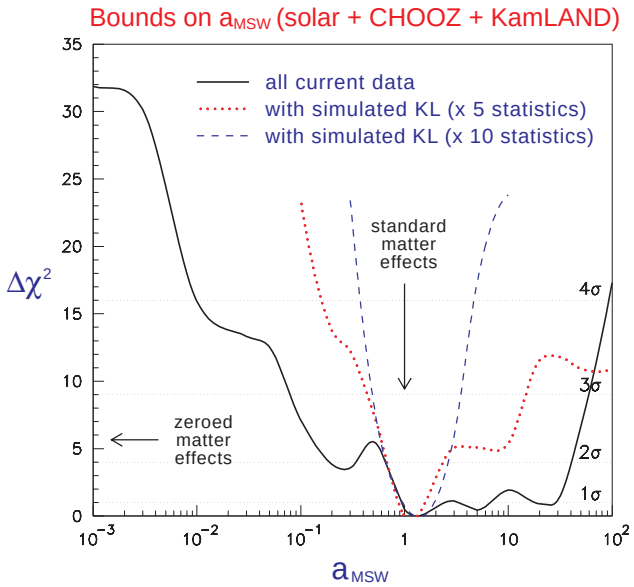

Figure 5: Bounds on $a_{\rm MSW}$ (considered as a continuous free parameter), including all current solar, CHOOZ, and KamLAND data (solid curve). Prospective KamLAND data with higher statistics are used to draw the dotted and dashed curves. See the text for details.

of $\mathcal{H}_{\rm dyn}$ independently of $\mathcal{H}_{\rm kin}$. It can be seen that the best fit is intriguingly close to the standard case ($a_{\rm MSW} = 1$), although there are other acceptable local minima over about three decades in $a_{\rm MSW}$. As discussed in [25] for the case of variable $a_{\rm MSW}$, the δm^2 range allowed by solar neutrino data sweeps through the tower of LMA-n solutions allowed by KamLAND, leading to a series of "bumps" in the $\Delta\chi^2$ function (solid line). Such features are unavoidable, as far as KamLAND allows multiple solutions in the mass-mixing parameter space. However, the situation should improve with higher KamLAND statistics. Assuming that KamLAND will confirm the current best-fit solution in the $(\delta m^2, \sin^2\theta_{12}, a_{\rm MSW})$ space, and simulating the corresponding KamLAND data, we obtain the prospective dotted and dahed curves in Fig. 5, which refer to a fivefold and tenfold increase of the present statistics (54 events [18]), respectively. It appears that, with the help of a few hundreds KamLAND events, the global fit of solar and reactor data can pinpoint the predicted size of MSW effects within a factor of ~ 2, allowing future "precision tests" of this effects (e.g., to probe additional nonstandard interactions).

Although the current bounds on $a_{\rm MSW}$ appear to be rather weak, the rejection of the null hypothesis $a_{\rm MSW} = 0$ is quite strong, and corresponds to a significance level of $\Delta\chi^2 \simeq 32$, i.e., $\sim 5.6\sigma$. Summarizing the results of this and the previous section, we can state that current solar and reactor data reject the hypothesis of no MSW effect at $> 5\sigma$ level, with a $> 3\sigma$ contribution from the recent SNO data [8]. Therefore, in our opinion, the phenomenological indications in favor of MSW effects can now be promoted to the level of evidence.

3.3 Constraints on kinematical mass-mixing term

In this subsection, assuming standard MSW dynamics, we update our previous bounds [20] on the mass-mixing parameters $(\delta m^2, \sin^2\theta_{12})$ which govern the kinematical term $\mathcal{H}_{\rm kin}$. The reader is referred to [20, 30] for technical details. Here we just add that the statistical correlations of recent SNO data [33] are incorporated through a straightforward generalization of the pull approach [30], as explicitly described in [37]. We have checked that our analysis "SNO data only" reproduces the results of [20] with very good accuracy. Finally, we have updated the total rate and winter-summer asymmetry from Gallium experiments [38]. In total, we have 84 solar neutrino observables, plus 13 KamLAND bins.

Figure 6 shows the results of our fit to all solar neutrino data, with a comparison with the fit before the inclusion of the last SNO data [8]. In the analysis on the right, also the CHOOZ data are added, in order to strengthen the upper bound on δm^2. Conversely, current solar neutrino data make this addition no longer necessary in the context of 2ν mixing with standard MSW effects. The best fit on the left side ($\chi^2_{\rm min} = 72.9$) is reached at $\delta m^2 = 5.7 \times 10^{-5}$ and $\sin^2\theta_{12} = 0.29$. The upper and lower bounds on the mass-mixing parameters are in good agreement with the results in [8], and confirm that the solar neutrino parameter space is steadily narrowing.

Figure 7 incorporates the analysis of KamLAND data [18] as in [20]. The best fit ($\chi^2_{\rm min} = 79.7$) is reached at $\delta m^2 = 7.2 \times 10^{-5}$ and $\sin^2\theta_{12} = 0.29$ (LMA-I solution), while the second best fit (LMA-II solution) is only marginally allowed at the $\Delta\chi^2 = 9.4$ level ($\sim 99\%$ C.L. for $N_{\rm DF} = 2$). Also in this case, we find good agreement with the results in

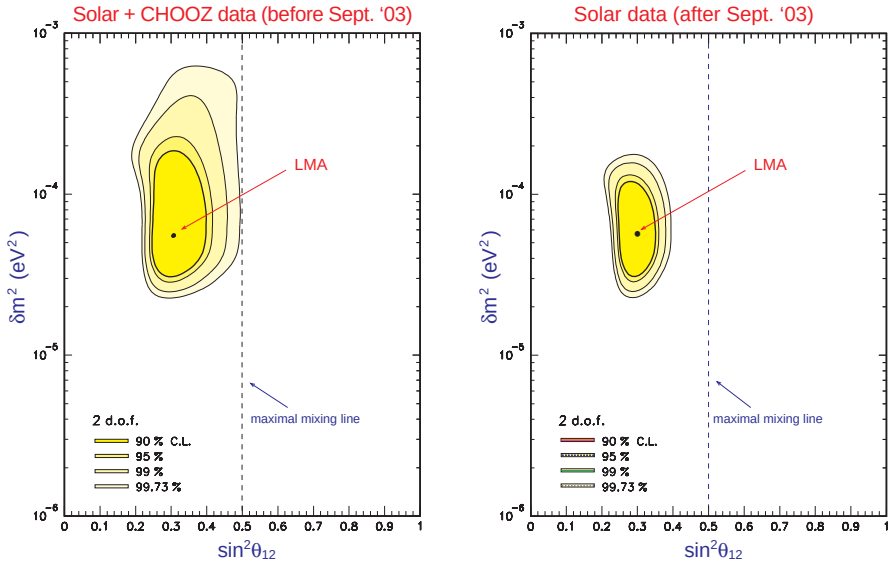

Figure 6: Two-flavor active neutrino oscillations, for standard MSW effects. On the left, global analysis of solar and CHOOZ neutrino data in the $(\delta m^2, \sin^2\theta_{12})$ parameter space, restricted to the LMA region, without including the last data from SNO. On the right, the global analysis including all the present solar neutrino data, in particular the last SNO results. The best fit is indicated by a black dot.

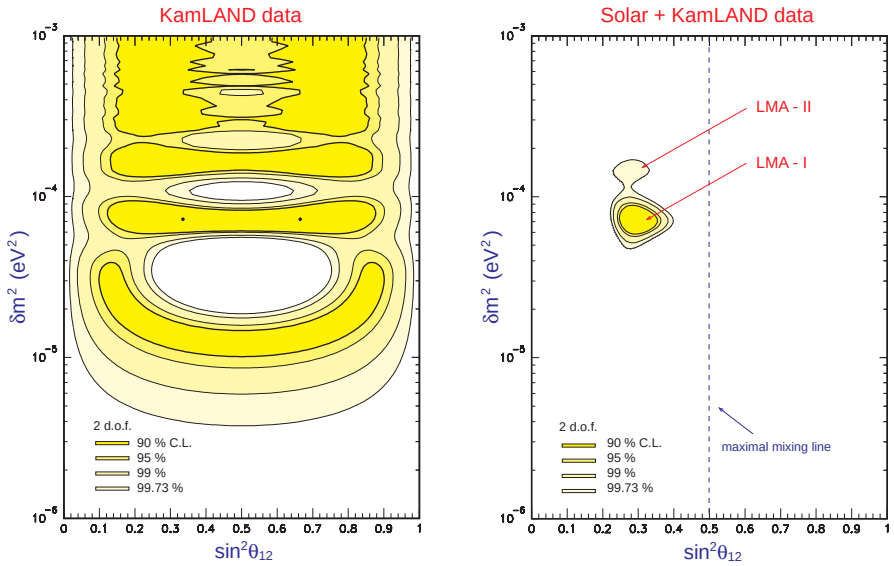

Figure 7: Two-flavor active neutrino oscillations, for standard MSW effects. On the left, global analysis of KamLAND data in the $(\delta m^2, \sin^2\theta_{12})$ parameter space. On the right, global analysis of solar and KamLAND neutrino data. As an effect of the last SNO data, the LMA region is significantly restricted and, of the two subregions (LMA-I and LMA-II), LMA-II is only marginally allowed. The best fits are indicated by a black dot.

[8], modulo the obvious transformation from our linear abscissa $\sin^2\theta_{12}$ to their logarithmic abscissa $\tan^2\theta_{12}$.

In conclusion, the kinematical 2ν mass-mixing parameters appear to be strongly constrained in a basically unique region (LMA-I), with only a marginal possibility left for the LMA-II region. The decrease of the previous LMA-II likelihood [20] is an important contribution of the latest SNO data [8].

4. Comments on three-family mixing

So far, we have assumed solar ν flavor oscillations in the active 2ν channel $\nu_e \to \nu_a$ (ν_a being a linear combination of ν_μ and ν_τ) driven by the $(\delta m^2, \theta_{12})$ parameters. The (ν_μ, ν_τ) combination orthogonal to ν_a is probed by atmospheric $\nu_\mu \to \nu_\tau$ oscillations, with different parameters $(\Delta m^2, \theta_{23})$ [39]. As far as the third mixing angle θ_{13} is zero (and $\delta m^2/\Delta m^2 \ll 1$), the two oscillation channels are practically decoupled, and all our previous considerations hold without changes. However, for small but nonzero θ_{13}, the 3ν survival probability deviates from the 2ν case for both solar and KamLAND ν_e oscillations:

$$P_{ee}^{3\nu} \simeq (1 - 2\sin^2\theta_{13}) P_{ee}^{2\nu} \ . \tag{4.1}$$

Concerning θ_{13}, until very recently the upper bound on θ_{13} (dominated by CHOOZ and atmospheric data) could be quoted as $\sin^2\theta_{13} < 0.05$ (3σ) [20], leading to $P_{ee}^{3\nu}(a_{\rm MSW} = 0) > 0.45$. A new SK atmospheric data analysis [40], however, appears to imply the weaker bound $\sin^2\theta_{13} < 0.067$ (3σ) [41], leading to $P_{ee}^{3\nu}(a_{\rm MSW} = 0) > 0.43$. In both cases, there is no overlap with the experimental upper bound of Eq. (3.6). Therefore, the null hypothesis $a_{\rm MSW} = 0$ can be rejected at the 3σ level also in the 3ν mixing case, using only SNO(+SK) data.

In the more general case of variable $a_{\rm MSW}$, we have not performed the 3ν generalization of the analysis in Subsec. 3.2. Our educated guess is that an allowance for small values of θ_{13} should only slightly weaken—but should not spoil—the main results discussed therein.

5. Conclusions

We have analyzed in detail the current SK atmospheric neutrino data and and the first K2K spectral data, in order to review the status of standard $\nu_\mu \to \nu_\tau$ oscillations. We have then provided updated bounds for the standard oscillation parameters. In particular, the statistical analysis of the uncertainties reveals that K2K will lead further progress in this field, especially through higher-statistics tests of the low-energy spectrum bins.

Going to solar neutrinos, we have pointed out that recent SNO data [8] strongly favor the occurrence of MSW effects in the solar matter and, together with world solar and reactor data, provide a many-sigma rejection of the null hypothesis. We have also performed an analysis where the MSW interaction energy is freely rescaled, and found poor constraints on the scaling parameter. These constraints can be potentially improved by higher-statistics KamLAND data, which will then allow more precise tests of the MSW dynamics. In the standard MSW case, we have also performed an updated analysis of two-family active oscillations of solar and reactor neutrinos.

We conclude by observing that, although MSW effects are an unavoidable consequence of the standard theory of electroweak interactions, their basic confirmation in the current neutrino phenomenology represents an important and reassuring experimental accomplishment, which strengthen our confidence in the emerging picture of neutrino masses and mixings.

6. Acknowledgments

G.L.F. thanks the organizers of the Conference for the kind ospitality. This work is supported in part by the Istituto Nazionale di Fisica Nucleare (INFN) and by the Italian Ministry of Education (MIUR) through the "Astroparticle Physics" project.

References

[1] SK Collaboration, Y. Fukuda *et al.*, Phys. Rev. Lett. **81**, 1562 (1998) [hep-ex/9807003].

[2] T. Kajita and Y. Totsuka, Rev. Mod. Phys. **73**, 85 (2001).

[3] SK Collaboration, M. Shiozawa *et al.*,, in *Neutrino 2002,* Proceedings of the 20th International Conference on Neutrino Physics and Astrophysics (Munich, Germany, 2002), to appear.

[4] MACRO Collaboration, M. Ambrosio *et al.*, Phys. Lett. B **517**, 59 (2001).

[5] Soudan 2 Collaboration, W.W. Allison *et al.*, Phys. Lett. B **449**, 137 (1999).

[6] K2K Collaboration, S.H. Ahn *et al.*, Phys. Lett. B **511**, 178 (2001).

[7] K2K Collaboration, M.H. Ahn *et al.*, Phys. Rev. Lett. **90**, 041801 (2003).

[8] SNO Collaboration, S.N. Ahmed *et al.*, nucl-ex/0309004, submitted to Phys. Rev. Lett.

[9] Homestake Collaboration, B.T. Cleveland, T. Daily, R. Davis Jr., J.R. Distel, K. Lande, C.K. Lee, P.S. Wildenhain, and J. Ullman, Astrophys. J. **496**, 505 (1998).

[10] SAGE Collaboration, J.N. Abdurashitov *et al.*, J. Exp. Theor. Phys. **95**, 181 (2002) [Zh. Eksp. Teor. Fiz. **95**, 211 (2002)].

[11] GALLEX Collaboration, W. Hampel *et al.*, Phys. Lett. B **447**, 127 (1999).

[12] T. Kirsten for the GNO Collaboration, in *Neutrino 2002*, 20th International Conference on Neutrino Physics and Astrophysics (Munich, Germany, 2002).

[13] SK Collaboration, S. Fukuda *et al.*, Phys. Rev. Lett. **86**, 5651 (2001); *ibidem*, 5656 (2001).

[14] SK Collaboration, S. Fukuda *et al.*, Phys. Lett. B **539**, 179 (2002).

[15] SNO Collaboration, Q.R. Ahmad *et al.*, Phys. Rev. Lett. **87**, 071301 (2001).

[16] SNO Collaboration, Q.R. Ahmad *et al.*, Phys. Rev. Lett. **89**, 011301 (2002).

[17] SNO Collaboration, Q.R. Ahmad *et al.*, Phys. Rev. Lett. **89**, 011302 (2002).

[18] KamLAND Collaboration, K. Eguchi *et al.*, Phys. Rev. Lett. **90**, 021802 (2003).

[19] CHOOZ Collaboration, M. Apollonio *et al.*, Phys. Lett. B **466**, 415 (1999); M. Apollonio *et al.*, Eur. Phys. J. C. **27**, 331 (2003).

[20] G.L. Fogli, E. Lisi, A. Marrone, D. Montanino, A. Palazzo, and A. Rotunno, Phys. Rev. D. **67**, 073002 (2003).

[21] J. N. Bahcall, M. C. Gonzalez-Garcia, and C. Peña-Garay, JHEP **0302**, 009 (2003).

[22] L. Wolfenstein, Phys. Rev. D **17**, 2369 (1978); S.P. Mikheev and A.Yu. Smirnov, Yad. Fiz. **42**, 1441 (1985) [Sov. J. Nucl. Phys. **42**, 913 (1985)].

[23] V.D. Barger, K. Whisnant, S. Pakvasa, and R.J.N. Phillips, Phys. Rev. D **22**, 2718 (1980).

[24] L. Wolfenstein, in *Neutrino '78*, 8th International Conference on Neutrino Physics and Astrophysics (Purdue U., West Lafayette, Indiana, 1978), ed. by E.C. Fowler (Purdue U. Press, 1978), p. C3.

[25] G.L. Fogli, E. Lisi, A. Palazzo, and A.M. Rotunno, Phys. Rev. D **67**, 073001 (2003).

[26] G.L. Fogli, E. Lisi, A. Marrone and D. Montanino, Phys. Rev. D **67**, 093006 (2003)

[27] G.L. Fogli, E. Lisi, A. Marrone, and G. Scioscia, Phys. Rev. D **59**, 033001 (1999).

[28] G.L. Fogli, E. Lisi, and A. Marrone, Phys. Rev. D **64**, 093005 (2001).

[29] G.L. Fogli, E. Lisi, and A. Marrone, Phys. Rev. D **65**, 073028 (2002).

[30] G.L. Fogli, E. Lisi, A. Marrone, D. Montanino and A. Palazzo, Phys. Rev. D **66**, 053010 (2002).

[31] G.L. Fogli, G. Lettera, E. Lisi, A. Marrone, A. Palazzo, and A. Rotunno, Phys. Rev. D **66**, 093008 (2002).

[32] F.L. Villante, G. Fiorentini, and E. Lisi, Phys. Rev. D **59**, 013006 (1999).

[33] SNO Collaboration, "How to use the SNO Salt flux results", available at www.sno.phy.queensu.ca

[34] J.N. Bahcall, M.H. Pinsonneault, and S. Basu, Astrophys. J. **555**, 990 (2001).

[35] M. Maris and S.T. Petcov, Phys. Lett. B **534**, 17 (2002).

[36] P.C. de Holanda and A. Yu. Smirnov, JCAP **0302**, 001 (2003).

[37] A.B. Balantekin and H. Yuksel, JCAP **0302**, 001 (2003).

[38] E. Bellotti and V. Gavrin, talks at LowNu 2003 (Paris, France, 2003), available at cdfinfo.in2p3.fr/LowNu2003

[39] See, e.g., the reviews: S.M. Bilenky, C. Giunti, and W. Grimus, Prog. Part. Nucl. Phys. **43**, 1 (1999); P. Langacker, in *NOW 2000*, Proceedings of the Neutrino Oscillation Workshop 2000 (Conca Specchiulla, Italy, 2000), ed. by G.L. Fogli, Nucl. Phys. Proc. Suppl. **100**, 383 (2001); M. C. Gonzalez-Garcia and Y. Nir, Rev. Mod. Phys. 75, 345 (2003).

[40] Y. Hayato, *"Status of the Super-Kamiokande, the K2K and the J-Park ν project"*, talk at *HEP 2003*, International Europhysics Conference on High Energy Physics (Aachen, Germany, 2003). Website: eps2003.physik.rwth-aachen.de

[41] G.L. Fogli, E. Lisi, A. Marrone, D. Montanino, A. Palazzo, and A. Rotunno, hep-ph/0308055.